Density Embedding Method for Nanoscale Molecule−Metal Interfaces

Xuecheng Shao,* Wenhui Mi,* and Michele Pavanello*

Read Online

ACCESS | Metrics & More | Article Recommendations | Supporting Information

ABSTRACT: In this work, we extend the applicability of standard Kohn−Sham DFT (KS-DFT) to model realistically sized molecule−metal interfaces where the metal slabs venture into the tens of nanometers in size. Employing state-of-the-art noninteracting kinetic energy functionals, we describe metallic subsystems with orbital-free DFT and combine their electronic structure with molecular subsystems computed at the KS-DFT level resulting in a multiscale subsystem DFT method. The method reproduces within a few millielectronvolts the binding energy difference of water and carbon dioxide molecules adsorbed on the top and hollow sites of an Al(111) surface compared to KS-DFT of the combined supersystem. It is also robust for Born−Oppenheimer molecular dynamics simulations. Very large system sizes are approached with standard computing resources thanks to a parallelization scheme that avoids accumulation of memory at the gather−scatter stage. The results as presented are encouraging and open the door to ab initio simulations of realistically sized, mesoscopic molecule−metal interfaces.
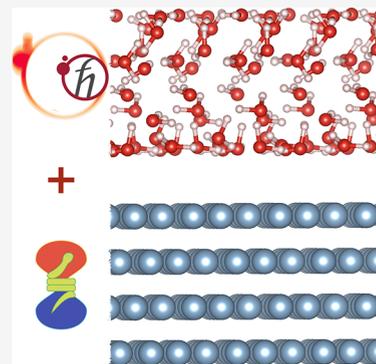
Density Functional Theory (DFT) and specifically Kohn−Sham DFT (KS-DFT) dominate the landscape of ab initio computational chemistry and materials science.[1,2] The low computational cost compared to accurate quantum chemical methods and the retained accuracy make KS-DFT the method of choice for most chemistry, physics and material science applications.

The computational cost of standard KS-DFT implementations is proportional to N^3, where N is a measure of the system size.[3] While this is generally excellent, it in fact restricts the application of DFT to systems of reduced size (generally 1−2 nm). So far, such a limitation has not stopped modelers from using KS-DFT in predictive ways. They typically formulate model systems of much reduced sizes compared to realistic systems but still of significance so that useful predictions can be extracted from the models. Given this background, it is not surprising that, besides the unavoidable approximations intrinsic in practical implementations of KS-DFT[4] (i.e., the need to employ approximate exchange−correlation functionals), one of the errors typically invoked in DFT simulations is finite-size effects. These arise when the systems afforded by the modeler are still too small to provide an accurate description. Finite-size effects in computational material science were identified almost at DFT's conception[5] and are still very much a subject of work toward finding mitigating corrections and workarounds.[6,7]

To attack the computational scaling problem of KS-DFT, several avenues of research are being pursued, involving divide and conquer[8−14] as well as many-body expansions[15−25] and real-space methods[3,26−42] which can be used in conjunction with ideas of embedding.[41,42]

In this work, we also subscribe to the concept of divide and conquer by advancing the method of density embedding also known as subsystem DFT (sDFT). sDFT was popularized by Wesolowski and Warshel in 1993[43] with antecedents by Senatore and Subbaswamy[44] as well as Cortona.[45] sDFT prescribes to split the system into smaller, interacting subsystems, i.e., the electron density is given by the sum of the subsystem electron densities,

$$\rho(\mathbf{r}) = \sum_{I=1}^{N_S} \rho_I(\mathbf{r})$$

(1)

the energy functional given by subsystem additive and nonadditive parts,

$$E[\{\rho_I, v_{ext}^I\}] = \sum_{I=1}^{N_S} E[\rho_I, v_{ext}^I] + E^{nad}[\{\rho_I, v_{ext}^I\}]$$

(2)

The additive term is comprised of the sum of ground-state functionals of the electron densities of the subsystems. The nonadditive term, E^{nad}, includes Coulomb interactions among electrons and nuclei of different subsystems as well as the nonadditive exchange−correlation (xc) and noninteracting
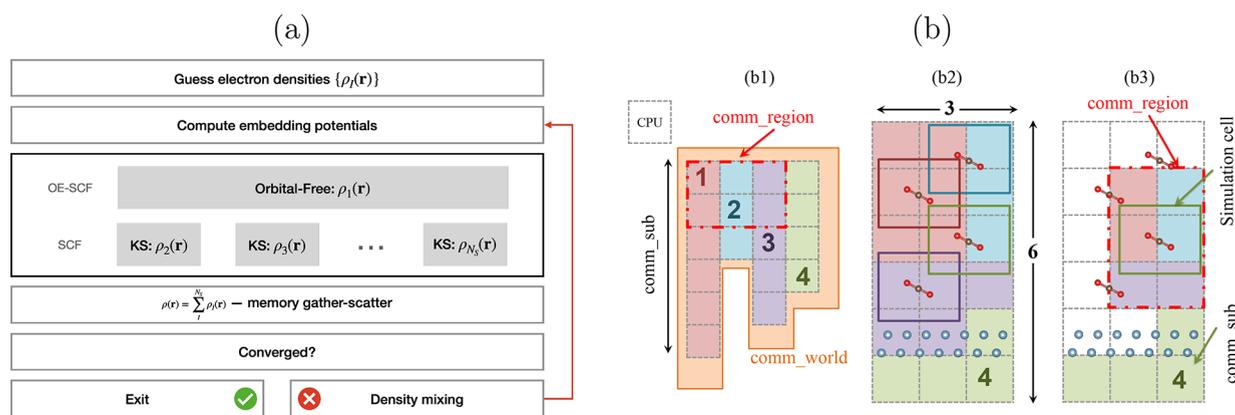
Figure 1. (a) Workflow of a single SCF cycle of the proposed method. OF-DFT is used for the first subsystem to obtain the electron density $\rho_1(\mathbf{r})$. A KS-DFT solver (in this work, QE) is used for the other subsystems. The memory gather−scatter step is described in part b and is used to generate the total electron density from the subsystem ones. (b) Parallelization of work and data in eDFTpy. (b1) Work-related subsystem MPI communicators (`comm_sub`) which in this case handle four subsystems of different sizes, associated with six, three, five, and four MPI tasks for the four subsystems. (b2) Same communicators in the stack ordering of `comm_world` (i.e., `MPI_COMM_WORLD`) and also highlighting the spatial extend of the subsystems in the FFT grid. (b3) So-called "region" communicators (`comm_region`) which are used to handle the memory when gathering and scattering a subsystem density or potential on the global FFT grid which maps on `comm_world`. The use of `comm_region` avoids the gathering of global data on a single CPU, which would be unfeasible for large systems such as the ones we target with the proposed method.

kinetic energy functionals which we denote hereafter by NAXC and NAKE, respectively. They are defined as follows,

$$E_{xc}^{nad}[\{\rho_I\}] = E_{xc}[\rho] - \sum_{I=1}^{N_S} E_{xc}[\rho_I],$$

$$T_s^{nad}[\{\rho_I\}] = T_s[\rho] - \sum_{I=1}^{N_S} T_s[\rho_I] \tag{3}$$

sDFT is similar to KS-DFT in that it is exact in principle. However, in addition to KS-DFT, sDFT's practical implementations require the approximation of both NAXC and NAKE. For NAXC, one can borrow the same (pure) density functionals employed in KS-DFT implementations (such as local and semilocal functionals). For NAKE, the situation is more delicate, as we discuss later in this manuscript, where generally subsystems can only be weakly interacting in order to keep the simulations quantitatively close to a KS-DFT simulation of the entire system.[46−51] We refer the interested reader to several reviews on sDFT[52−56] for additional details.

In practice, the KS equations with constrained electron density are solved for each subsystem. Namely,

$$\left[-\frac{1}{2}\nabla^2 + v_s[\rho_I](\mathbf{r}) + v_{emb}^I(\mathbf{r}) \right] \phi_i^I(\mathbf{r}) = \varepsilon_i^I \phi_i^I(\mathbf{r}) \tag{4}$$

where the embedding potential, $v_{emb}^I(\mathbf{r})$, is given by

$$v_{emb}^I(\mathbf{r}) = v_H[\rho - \rho_I](\mathbf{r}) + \sum_{J \neq I} v_{ext}^J(\mathbf{r}) + v_{T_s}^{nad}(\mathbf{r}) + v_{xc}^{nad}(\mathbf{r}) \tag{5}$$

The potential terms with superscript *nad* refer to the functional derivatives with respect to ρ_I of the nonadditive functionals in eq 3. The external potential of subsystem J is indicated by $v_{ext}^J(\mathbf{r})$, and $v_H[\rho - \rho_I](\mathbf{r})$ is the electronic Hartree potential computed for the electron density of the subsystems in the environment, i.e., $\rho(\mathbf{r}) - \rho_I(\mathbf{r})$. Once eq 4 is solved, it is possible to reconstruct the new, updated subsystem electron densities by $\rho_I(\mathbf{r}) = \sum_i n_i \phi_i^I(\mathbf{r})$ where n_i are the occupation number associated with each subsystem KS orbital, $\phi_i^I(\mathbf{r})$. We

remark that, for sake of clarity in the presentation, we did not explicitly show k-point sampling. However, in our simulations, we have the capability to perform it.

A major issue in sDFT is the fact that subsystems can become large—and sometimes very large. For example, when dealing with interfaces such as the case of molecules at surfaces, the surface should be treated as a single subsystem. However, even considering subsystem-based electronic basis sets to expand the subsystem KS orbitals, ϕ_i^I, (sometimes referred to as "monomer basis"[57] and achieved also in plane wave basis sets by expanding the Hamiltonian of each subsystem as in eq 4 in a separate plane wave basis associated with reduced simulation cells[47,58]) and considering that the k-point sampling can be carried out exclusively for the surface and not for the molecular subsystems,[59] the computational cost associated with the surface overpowers all other subsystems. Therefore, even with sDFT at hand, simulations of realistically sized interface systems have been scarce.[60] In particular, in this work we focus on metal−molecule interfaces.

In recent years, orbital-free DFT (OF-DFT) has emerged as a useful electronic structure method for materials science applications,[61−63] for systems at equilibrium as well as out of equilibrium.[64−66] Simple metals and some semiconductors have been successfully modeled with OF-DFT for either bulk,[67−69] clusters,[70,71] or surfaces.[72,73] Thus, it is conceivable that OF-DFT can be employed as the electronic structure solver for metallic subsystems in a sDFT simulation keeping KS-DFT as the solver for molecular subsystems. Given the reported accuracy of OF-DFT for metals, we expect the resulting sDFT method to maintain an accuracy similar to standard sDFT (i.e., where KS-DFT is used for the metallic subsystem as well). However, and most importantly, OF-DFT would allow us to cut down significantly on the computational time to solution.

There are several implementations of sDFT which are suitable for molecular[57,74] and periodic systems.[58,75−77] Because of the emphasis on interfaces, we will be considering the so-called slab calculations,[78] which require taking into account periodicity in the horizontal plane. Therefore, for
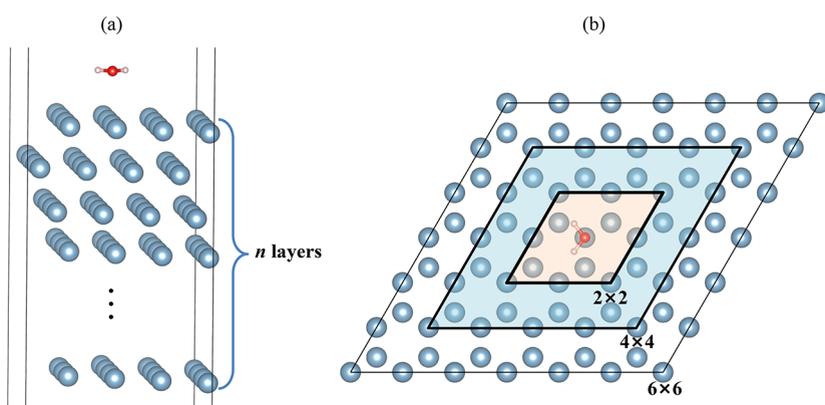
Figure 2. Systems considered in this work. (a) Single molecule of water on a 4×4 slab of Al(111) varying the number of layers in the slab from 1 to 100. (b) Single water molecule on a Al(111) surface of varying supercell dimensions, from 2×2 to 18×18.
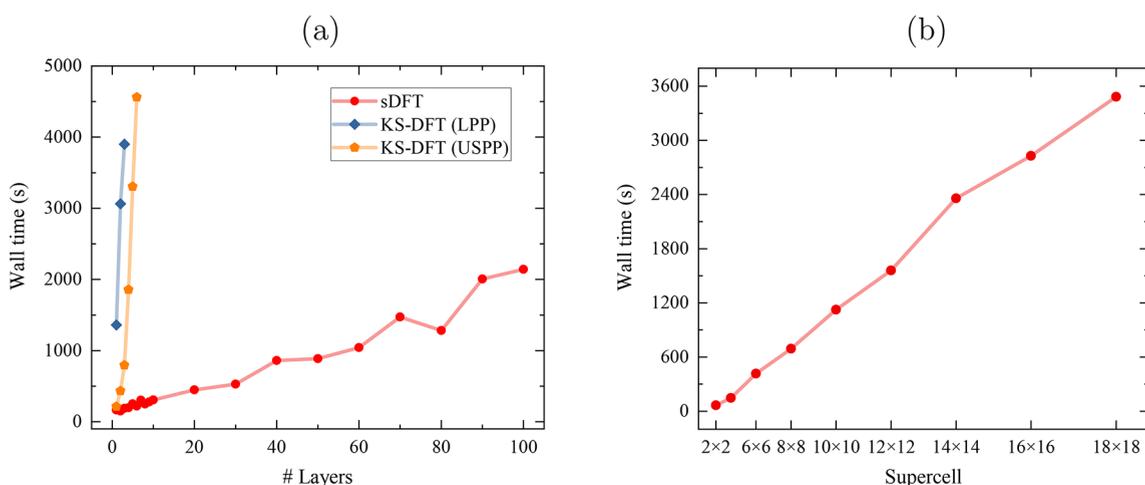
Figure 3. Timing to solution in seconds for the systems in Figure 2. Parts a and b are related to parts a and b of Figure 2. Surface area is measured in supercell size where $n \times n$ involves a supercell slab with n Al atoms along each of the two horizontal lattice vectors in each layer.

molecular systems, we use KS-DFT implemented in Quantum ESPRESSO (QE),[79] which we recently developed into an object-oriented Python code called QEpy.[80] For the metallic slab subsystems, we use OF-DFT implemented in DFTpy.[64]

The solvers for OF-DFT and KS-DFT are generally fundamentally different. OF-DFT solvers[81] variationally minimize the energy functional by real-space minimization (typically involving a line search algorithm) to find the electron density associated with minimum energy while constraining it to integrate to the number of electrons. KS-DFT solvers, instead, use the so-called self-consistent field (SCF) method. SCF is iterative, and rather than minimizing directly the energy functional, the KS equations [similar to eq 4] are solved by diagonalization of the KS Hamiltonian.

When combining OF-DFT with KS-DFT subsystems, one wishes the electronic structure solvers to be as similar as possible to produce an efficient, fast code. Therefore, typical OF-DFT solvers may not be compatible with an efficient sDFT implementation involving simultaneously OF-DFT and KS-DFT subsystems. Recently, however, our group formulated an iterative solver for OF-DFT called orbital ensemble SCF (OE-SCF) which is similar to the standard SCF but is specific to OF-DFT. In short, OE-SCF is iterative with respect to the Pauli, Hartree, and exchange−correlation potentials. These are kept fixed during a variational minimization. In doing so, the fixed potentials need to be evaluated only a handful of times

rather than hundreds or thousands of times when a conventional variational minimization is employed. Additional details about OE-SCF can be retrieved in the original publication.[62] The opportunity is in the possibility to update the embedding potentials for every SCF cycle for the KS-DFT subsystems, and every OE-SCF cycle for the OF-DFT subsystem. The resulting efficient algorithm is summarized in Figure 1a, while in Figure 1b we present a sketch of the parallelization scheme developed for this purpose in the in-house sDFT code eDFTpy.[82]

To describe the algorithm, we assume each subsystem starts with an initial guess electron density. For the OF-DFT subsystem, we begin from an electron density given as the sum of atomic contributions. For the KS-DFT subsystems, we rely on the QE initial guess, which is a combination of atomic contributions and contributions from random wave functions. First, the OF-DFT subsystem carries out a single OE-SCF cycle utilizing the entire number of CPUs available in the `comm_world` MPI communicator (MPI stands for Message Passing Interface). Then, the KS-DFT subsystems split the available CPUs (or CPU cores) according to user input (each subsystem uses the `comm_sub` subsystem communicators to carry out the work simultaneously). Once the SCF cycle is complete in each KS-DFT subsystem, the electron densities are broadcast to the global system simulation cell which is mapped onto the `comm_world` MPI communicator. At that stage, if

Table 1. Binding Energies (E_B, Computed as the Sum of the Energies of Isolated Molecule and Slab Removed of the Energy of the Interacting Molecule + Slab system) of H_2O and CO_2 Deposited on the Top (*top*) and Hollow (*hol*) Site of the Al(111) Surface, Varying the Number of Surface Layers (n)[a]

system	method	NAKE	E_B^{top} (meV)					$E_B^{top} - E_B^{hol}$ (meV)				
			$n=1$	$n=2$	$n=3$	$n=4$	$n=40$	$n=1$	$n=2$	$n=3$	$n=4$	$n=40$
H_2O	sDFT	revAPBEK	81	74	70	70	69	57	54	50	47	53
		LMGP	40	34	33	30	30	52	48	49	49	45
	KS-DFT		29	−16	−11	8	−	80	74	70	71	−
CO_2	sDFT	revAPBEK	−111	−111	−109	−109	−108	−45	−44	−44	−46	−44
		LMGP	−181	−181	−180	−181	−181	−44	−42	−43	−45	−44
	KS-DFT		−351	−356	−327	−324	−	−48	−41	−36	−35	−

[a]The relative stability of the top and hollow adsorption sites is also given. The calculations are labelled sDFT for our new subsystem DFT method and KS-DFT for the calculation of the full system with QE employing the effective local pseudopotentials for the Al ions (LPP). Results computed with ultrasoft pseudopotentials (USPP) are available in the Supporting Information.

it is determined that the electronic structure has not converged, the electron densities are sent to the DIIS mixer,[83] then potentials are updated, and finally, they are fed back to the SCF cycle.

The key to obtain efficient timings of execution is in the load balancing of the resources (optimal number of CPUs to each KS-DFT subsystem). Therefore, the algorithm needs to be able to (1) run the simulations with a custom number of CPUs for each KS-DFT subsystem. This can be achieved in eDFTpy and embedded QE package (eQE[58,76]) by user input. However, eQE does not support OF-DFT subsystems. (2) Due to the possibility of approaching very large system sizes, handling the parallelization of data (memory) is particularly complicated. For example, the memory handling developed previously by us in eQE relies on gathering the data of each subsystem communicator onto a single processor which allocates the simulation cell of the entire system. This would not be appropriate here because due to the large system sizes considered the memory requirement to allocate the full simulation cell is simply not available to a single process (or single compute node). For this reason we developed a completely new parallelization scheme (described in Figure 1b) that, by defining physical regions of space and associating to them "region" MPI communicators (`comm_region`), completely avoids gathering data of the entire system on single processors. Data gathering only occurs within a region, and a specially built map copies the data from the region to arrays handled by `comm_world`.

We present computational timings to solution for three model systems which, due to their size, are completely inaccessible to mainstream KS-DFT methods. However, we show that with our method, they are within reach of commonplace computational resources available to most researchers. Figure 2 depicts two of the systems considered which consist of a single water molecule deposited on top of an Al(111) surface of different sizes in terms of thickness or surface area. In Figure 3 we report the associated wall times to solution in comparison to (where available) KS-DFT carried out by QE. The Methods lists the computational details of the simulations. The figure shows that the new sDFT method scales almost linearly with system size, while the KS-DFT method (represented here by QE) scales much more steeply. Specifically, the time needed by QE to compute a water on a 4-layer Al(111) system is twice as the time needed by sDFT to compute water on a slab of 100 layers Al(111) using the same computational resources! We reach a similar conclusion when

varying the surface area; i.e., sDFT reaches linear-scaling times to solution with respect to the slab surface area.

Even though the dimensionalities reached by our method are generally outside of mainstream KS-DFT solvers, for small system sizes, we can carry out KS-DFT simulations of the entire system using QE which we can use as a benchmark of accuracy. There are two aspects of our simulations that make them more approximate compared to KS-DFT: i.e., we use pure density functionals for computing the electronic structure of the metallic slab as well as the interaction among subsystems. Thus, we compare our simulations against KS-DFT results (i.e., KS-DFT is the benchmark) computed with QE for the entire system for a few model systems of small size. In Table 1, we show the binding energy in millielectronvolts of water and CO_2 on the top and hollow sites of the Al(111) surface with a varying number of layers in the metal slab. We list the computational details in the Methods. In Table S1 in the Supporting Information, we also report sDFT results with the Al surface computed at the KS-DFT level.

We note that our method, labeled sDFT, produces binding energies that agree with the benchmark to within 100 to 150 meV which is the generally accepted accuracy of DFT simulations for the type of systems considered. Inspecting the results for the binding energies of the top adsorption site for water, we note that the KS-DFT benchmark predicts a binding energy that is positive for 1 and 4 Al surface layers, but is negative for 2 and 3 layers. sDFT predicts all binding energies to be positive. This is not too concerning because the KS-DFT binding energies with negative values are very small in magnitude (up to −16 meV).

Particularly significant is the fact that our sDFT method can reproduce very accurately the relative stability of the adsorbates on the top and hollow sites. These are not trivial quantities to reproduce, especially considering that for water the top adsorption site is more stable than the hollow site, while for carbon dioxide is the opposite. As expected, comparing the performance of the semilocal revAPBEK and the nonlocal LMGP NAKE functionals, we see that LMGP brings the sDFT result much closer to the KS-DFT benchmark. This is expected because LMGP was shown to be superior to revAPBEK in reproducing weak intermolecular interactions.[46,48]

We should remark that sDFT constrains the number of electrons in each subsystem to remain constant throughout the SCF procedure. Therefore, our method is expected to become approximate whenever there is a strong molecule−metal charge transfer. We also remark that even though we do not

consider corrections for the inclusion of van der Waals interactions (which are typically missed by GGA exchange–correlation functionals, such as PBE) our analysis is still meaningful as a van der Waals correction would only apply to the exchange–correlation functional while in our method, the functional under scrutiny is the noninteracting kinetic energy, $T_s[\rho]$.

In Table S2 of the Supporting Information document we also report values of dipole moments computed along the vertical, z, direction for molecule, metal surface, and the combined system molecule + metal surface. The sDFT dipole moments (whether with the surface computed with OF-DFT or with KS-DFT) are in good agreement with the values computed with KS-DFT of the combined molecule + metal system. For both water and CO_2, we note that the surface dipole partially cancels out the molecular dipole. Also, for water the z dipole for the top adsorption site is larger in magnitude compared to the hollow adsorption site. For CO_2, the dipole, instead, increases in magnitude. Such behavior is captured by sDFT.

In Figure 4, we report total energies calculated with KS-DFT and sDFT (with two NAKE functionals) along an NVT BO
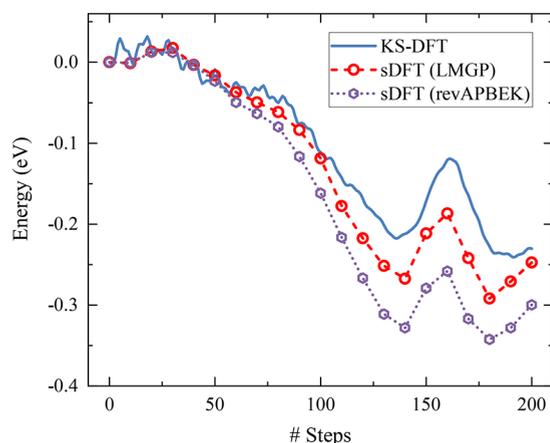
Figure 4. Total energies along a 200-step NVT BO dynamics carried out with KS-DFT for a water molecule on a frozen monolayer Al(111) surface sampling geometries beyond the top and hollow adsorption sites. KS-DFT (blue solid line). sDFT energies are computed with revAPBEK and LMGP NAKE functionals (dotted and dashed lines) and are evaluated every 10 steps (20 structures in total).

dynamics. The figure shows that sDFT recovers the correct energy landscape, including energy local minima and local maxima. Even though the agreement is within about 50 meV when LMGP NAKE is used and 100 meV when revAPBEK is used, the fact that sDFT recovers the correct energy landscape is of note and shows that the new method if applied to BO dynamics simulations for this system would produce predictive results. In the Supporting Information, Figure S1, we also show that a 100-step NVE BO dynamics carried out with the new sDFT method for water on a 10-layer Al(111) surface conserves the total energy along the dynamics with a small energy drift of 3 (meV/atom)/ps.

Finally, to show the capabilities of our method for modeling more realistic interfaces, we model wet aluminum surfaces by considering a 4-layer slab of Al(111) solvated by a multitude of water molecules. We start from a system containing 256 water molecules and increase to 640 water molecules simply by increasing the surface area of the slab and including a

proportional number of water molecules in the system. In part a of Figure 5, we show a snapshot of the system, and in part b, we report the wall time and parallel efficiency.

Inspecting the wall times for the systems in the figure, we notice they are all very small, less than 150 s. Given the system sizes considered, this is to be considered a very successful test. Additionally, the parallel efficiency (probing the parallel scalability of the code) shows that in going from 512 to 1280 cores the loss is merely 20%. Once again, this indicates a very successful test of efficiency for our implementation and algorithm. Even with a fairly modest set of CPU cores, it is possible to run simulations of such large system sizes in wall times that would support carrying out converged Born–Oppenheimer dynamics simulations within a reasonable time window.

In conclusion, we presented a new subsystem DFT method tailored to model molecule–metal interfaces. We show that massive computational savings can be achieved by employing orbital-free DFT as the electronic structure solver for metallic subsystems without compromising on the accuracy of the results. Specifically, by employing a new-generation nonlocal noninteracting kinetic energy functional, LMGP, as both the electronic structure solver for the metallic subsystems and as the nonadditive kinetic energy functional, the accuracy of the subsystem DFT simulations approach the parent Kohn–Sham DFT of the combined total system for model systems comprised of adsorbed water and CO_2 on Al(111) with varying slab layer number and surface area. With the resulting, new subsystem DFT method, we find a linear computational scaling in the limiting cases of many metal slab layers (up to 100 layers) as well as the metal slab surface area (up to 18×18 supercells), and we also show that a system composed of a wet 4-layer Al(111) surface slab solvated by 640 water molecules can be solved in less than 150 s employing 1280 CPU cores. The combination of KS-DFT and orbital-free DFT in a single electronic structure method is therefore useful in extending the applicability of DFT to interface system sizes of realistic sizes virtually with no loss of accuracy in the predictions. In the future, more work needs to be done to assess the applicability of the method to metals beyond aluminum and to other interface structures. Work along these lines is ongoing.

■ METHODS

The surfaces are modeled with at least 25 Å vacuum between periodic slabs. This ensures that the interactions between the studied systems and their periodic images are negligible along the z axis. All sDFT calculations were performed with eDFTpy, a Python-based density embedding software.[82] eDFTpy is based on the all-Python code implementing OF-DFT in a plane wave basis set, DFTpy.[64] All KS-DFT calculations were performed with the Quantum ESPRESSO (QE) package.[79] eDFTpy also employs QE for solving the electronic structure of the KS subsystems. However, to better integrate the Python codebase of eDFTpy, we developed a Python interface to QE, QEpy.[80] We use the revised Perdew–Burke–Ernzerhof (revPBE) exchange–correlation functional. Because we rely on OF-DFT to solve for the electronic structure of metallic subsystems, and for evaluating the interaction between subsystems with nonadditive functionals, we need to employ pure functionals of the electron density for the noninteracting kinetic energy. For this purpose, in this work, we use LMGP[70] and revAPBEK.[50] While revAPBEK is a GGA functional of straightforward evaluation (it depends only on the density and
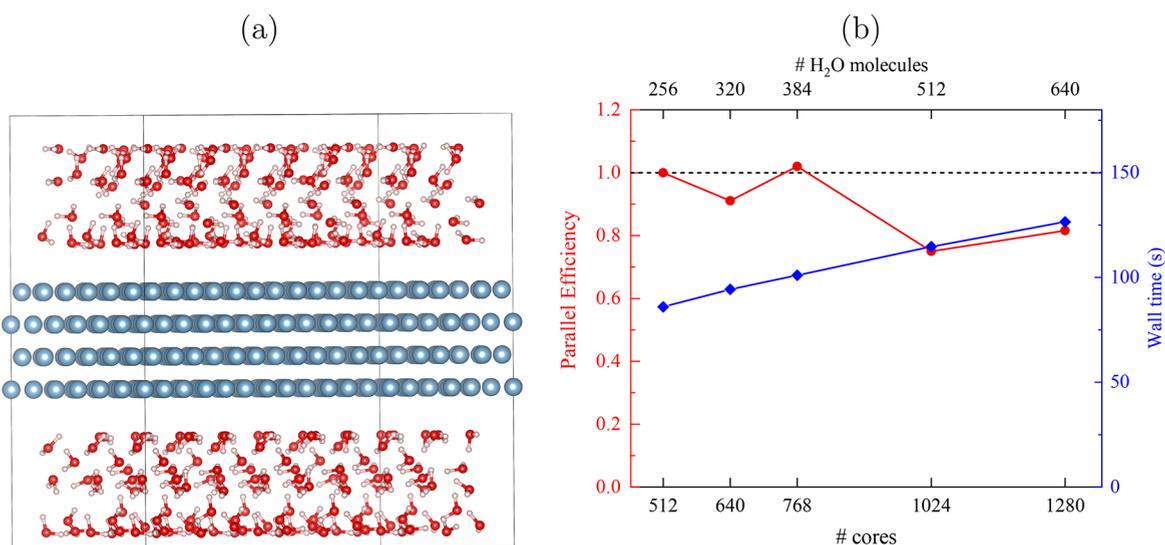
Figure 5. (a) Snapshot of the system considered as an example of multiple KS-DFT subsystems interacting with a OF-DFT metal slab. (b) Parallel efficiency (circles) and wall time (diamonds) when the system grows proportionally in Al(111) surface area and number of water molecule (top axis) as a function of the number of CPU cores employed in the simulations (bottom axis).

its gradient), LMGP is a nonlocal functional with density-dependent kernel whose evaluation requires specialized software implementations which are available in DFTpy, eDFTpy, and eQE.[62,64,76] revAPBEK was only used as nonadditive functional. The GBRV ultrasoft pseudopotentials (USPP) are adopted for KS-DFT. In KS-DFT calculations, the kinetic energy cutoffs of wave function and density are 40 and 400 Ry, respectively, and a $9 \times 9 \times 1$ k-point mesh is used. When OF-DFT is used as a solver for the Al(111) surfaces, we use the bulk-derived local pseudopotentials (LPP)[84] and a cutoff of 200 Ry. In Figure 3a and Tables 1, S1, and S2 we also use the LPP as the Al pseudopotential in KS-DFT, and we adopt plane wave cutoffs of 100 and 400 Ry for wave functions and density, respectively.

ASSOCIATED CONTENT

ⓢ Supporting Information

The Supporting Information is available free of charge at https://pubs.acs.org/doi/10.1021/acs.jpclett.2c01424.

> Table S1, extension of the data of Table 1 to include KS-DFT with different pseudopotentials and sDFT carried out with KS-in-KS; Table S2, molecular and surface dipole moments computed with KS-DFT and sDFT; and Figure S1, potential and total (conserved) energy along an *NVE* dynamics carried out with sDFT. (PDF)

AUTHOR INFORMATION

Corresponding Authors

Xuecheng Shao — *Department of Chemistry, Rutgers University, Newark, New Jersey 07102, United States;* ⓞ orcid.org/0000-0003-2215-0926; Email: xuecheng.shao@rutgers.edu

Wenhui Mi — *International Center for Computational Method and Software, College of Physics, Jilin University, Changchun 130012, China;* ⓞ orcid.org/0000-0002-1612-5292; Email: mwh@jlu.edu.cn

Michele Pavanello — *Department of Chemistry and Department of Physics, Rutgers University, Newark, New Jersey 07102, United States;* ⓞ orcid.org/0000-0001-8294-7481; Email: m.pavanello@rutgers.edu

Complete contact information is available at:
https://pubs.acs.org/10.1021/acs.jpclett.2c01424

Notes

The authors declare no competing financial interest.

■ REFERENCES

(1) Burke, K. Perspective on Density Functional Theory. *J. Chem. Phys.* **2012**, *136*, 150901.

(2) Maitra, N. T. Perspective: Fundamental aspects of time-dependent density functional theory. *J. Chem. Phys.* **2016**, *144*, 220901.

(3) Moussa, J. E.; Baczewski, A. D. Assessment of localized and randomized algorithms for electronic structure. *Electronic Structure* **2019**, *1*, 033001.

(4) Medvedev, M. G.; Bushmarinov, I. S.; Sun, J.; Perdew, J. P.; Lyssenko, K. A. Density functional theory is straying from the path toward the exact functional. *Science* **2017**, *355*, 49−52.

(5) Leslie, M.; Gillan, N. J. The energy and elastic dipole tensor of defects in ionic crystals calculated by the supercell method. *Journal of Physics C: Solid State Physics* **1985**, *18*, 973−982.

(6) Freysoldt, C.; Neugebauer, J.; Van de Walle, C. G. FullyAb InitioFinite-Size Corrections for Charged-Defect Supercell Calculations. *Phys. Rev. Lett.* **2009**, *102*, 016402.

(7) Freysoldt, C.; Grabowski, B.; Hickel, T.; Neugebauer, J.; Kresse, G.; Janotti, A.; Van de Walle, C. G. First-principles calculations for point defects in solids. *Rev. Mod. Phys.* **2014**, *86*, 253−305.

(8) Yang, W. Direct Calculation of Electron Density in Density-Functional Theory. *Phys. Rev. Lett.* **1991**, *66*, 1438−1441.

(9) Zhu, T.; Pan, W.; Yang, W. Divide-and-conquer calculations for clean surfaces and surface adsorption. *Theoretical Chemistry Accounts:*

Theory, Computation, and Modeling (Theoretica Chimica Acta) **1997**, *96*, 2−6.

(10) Akama, T.; Kobayashi, M.; Nakai, H. Implementation of divide-and-conquer method including Hartree-Fock exchange interaction. *J. Comput. Chem.* **2007**, *28*, 2003−2012.

(11) Kobayashi, M.; Akama, T.; Nakai, H. Second-order Møller-Plesset perturbation energy obtained from divide-and-conquer Hartree-Fock density matrix. *J. Chem. Phys.* **2006**, *125*, 204106.

(12) Fedorov, D. G.; Ishida, T.; Kitaura, K. Multilayer Formulation of the Fragment Molecular Orbital Method (FMO). *J. Phys. Chem. A* **2005**, *109*, 2638−2646.

(13) Fedorov, D. G.; Kitaura, K. Extending the Power of Quantum Chemistry to Large Systems with the Fragment Molecular Orbital Method. *J. Phys. Chem. A* **2007**, *111*, 6904−6914.

(14) Gordon, M. S.; Fedorov, D. G.; Pruitt, S. R.; Slipchenko, L. V. Fragmentation Methods: A Route to Accurate Calculations on Large Systems. *Chem. Rev.* **2012**, *112*, 632−672.

(15) Herbert, J. M. Fantasy versus reality in fragment-based quantum chemistry. *J. Chem. Phys.* **2019**, *151*, 170901.

(16) Bygrave, P. J.; Allan, N. L.; Manby, F. R. The embedded many-body expansion for energetics of molecular crystals. *J. Chem. Phys.* **2012**, *137*, 164102.

(17) Dahlke, E. E.; Truhlar, D. G. Electrostatically Embedded Many-Body Expansion for Large Systems, with Applications to Water Clusters. *J. Chem. Theory Comput.* **2007**, *3*, 46−53.

(18) Li, C.; Requist, R.; Gross, E. K. U. Density functional theory of electron transfer beyond the Born-Oppenheimer approximation: Case study of LiF. *J. Chem. Phys.* **2018**, *148*, 084110.

(19) Qi, H. W.; Leverentz, H. R.; Truhlar, D. G. Water 16-mers and Hexamers: Assessment of the Three-Body and Electrostatically Embedded Many-Body Approximations of the Correlation Energy or the Nonlocal Energy As Ways to Include Cooperative Effects. *J. Phys. Chem. A* **2013**, *117*, 4486−4499.

(20) Tempkin, J. O. B.; Leverentz, H. R.; Wang, B.; Truhlar, D. G. Screened Electrostatically Embedded Many-Body Method. The. *J. Phys. Chem. Lett.* **2011**, *2*, 2141−2144.

(21) Willow, S. Y.; Salim, M. A.; Kim, K. S.; Hirata, S. Ab initio molecular dynamics of liquid water using embedded-fragment second-order many-body perturbation theory towards its accurate property prediction. *Sci. Rep.* **2015**, *5*, 14358.

(22) Liu, Y.; Cheng, M.; He, Z.; Gu, B.; Xiao, C.; Zhou, T.; Guo, Z.; Liu, J.; He, H.; Ye, B.; et al. Pothole-rich Ultrathin WO3 Nanosheets that Trigger N≡N Bond Activation of Nitrogen for Direct Nitrate Photosynthesis. *Angew. Chem., Int. Ed.* **2019**, *58*, 731−735.

(23) Richard, R. M.; Lao, K. U.; Herbert, J. M. Aiming for Benchmark Accuracy with the Many-Body Expansion. *Acc. Chem. Res.* **2014**, *47*, 2828−2836.

(24) Lao, K. U.; Liu, K.-Y.; Richard, R. M.; Herbert, J. M. Understanding the many-body expansion for large systems. II.Accuracy considerations. *J. Chem. Phys.* **2016**, *144*, 164105.

(25) Liu, K.-Y.; Carter-Fenk, K.; Herbert, J. M. Self-consistent charge embedding at very low cost, with application to symmetry-adapted perturbation theory. *J. Chem. Phys.* **2019**, *151*, 031102.

(26) Baroni, S.; Giannozzi, P. Towards Very Large-Scale Electronic-Structure Calculations. *Europhysics Letters (EPL)* **1992**, *17*, 547−552.

(27) Li, X.-P.; Nunes, R. W.; Vanderbilt, D. Density-matrix electronic-structure method with linear system-size scaling. *Phys. Rev. B* **1993**, *47*, 10891−10894.

(28) Goedecker, S.; Colombo, L. Efficient Linear Scaling Algorithm for Tight-Binding Molecular Dynamics. *Phys. Rev. Lett.* **1994**, *73*, 122−125.

(29) Chelikowsky, J. R.; Troullier, N.; Saad, Y. Finite-difference-pseudopotential method: Electronic structure calculations without a basis. *Phys. Rev. Lett.* **1994**, *72*, 1240−1243.

(30) Kronik, L.; Makmal, A.; Tiago, M. L.; Alemany, M. M. G.; Jain, M.; Huang, X.; Saad, Y.; Chelikowsky, J. R. PARSEC − the pseudopotential algorithm for real-space electronic structure calculations: recent advances and novel applications to nano-structures. *physica status solidi (b)* **2006**, *243*, 1063−1079.

(31) Saad, Y.; Chelikowsky, J. R.; Shontz, S. M. Numerical Methods for Electronic Structure Calculations of Materials. *SIAM Review* **2010**, *52*, 3−54.

(32) Goedecker, S. Linear scaling electronic structure methods. *Rev. Mod. Phys.* **1999**, *71*, 1085−1123.

(33) Khaliullin, R. Z.; Kühne, T. D. Microscopic properties of liquid water from combined ab initio molecular dynamics and energy decomposition studies. *Phys. Chem. Chem. Phys.* **2013**, *15*, 15746.

(34) Shpiro, B.; Fabian, M. D.; Rabani, E.; Baer, R. Forces from stochastic density functional theory under nonorthogonal atom-centered basis sets. *J. Chem. Theory Comput.* **2022**, *18*, 1458−1466.

(35) Nguyen, M.; Li, W.; Li, Y.; Rabani, E.; Baer, R.; Neuhauser, D. Tempering stochastic density functional theory. *J. Chem. Phys.* **2021**, *155*, 204105.

(36) Chen, M.; Baer, R.; Neuhauser, D.; Rabani, E. Stochastic density functional theory: Real- and energy-space fragmentation for noise reduction. *J. Chem. Phys.* **2021**, *154*, 204108.

(37) Cytter, Y.; Rabani, E.; Neuhauser, D.; Preising, M.; Redmer, R.; Baer, R. Transition to metallization in warm dense helium-hydrogen mixtures using stochastic density functional theory within the Kubo-Greenwood formalism. *Phys. Rev. B* **2019**, *100*, 195101.

(38) Fabian, M. D.; Shpiro, B.; Rabani, E.; Neuhauser, D.; Baer, R. Stochastic density functional theory. *WIREs Computational Molecular Science* **2019**, *9*, 1412.

(39) Chen, M.; Baer, R.; Neuhauser, D.; Rabani, E. Energy window stochastic density functional theory. *J. Chem. Phys.* **2019**, *151*, 114116.

(40) Cytter, Y.; Rabani, E.; Neuhauser, D.; Baer, R. Stochastic density functional theory at finite temperatures. *Phys. Rev. B* **2018**, *97*, 115207.

(41) Chen, M.; Baer, R.; Neuhauser, D.; Rabani, E. Overlapped embedded fragment stochastic density functional theory for covalently-bonded materials. *J. Chem. Phys.* **2019**, *150*, 034106.

(42) Li, W.; Chen, M.; Rabani, E.; Baer, R.; Neuhauser, D. Stochastic embedding DFT: Theory and application to p-nitroaniline in water. *J. Chem. Phys.* **2019**, *151*, 174115.

(43) Wesolowski, T. A.; Warshel, A. Frozen Density Functional Approach for *ab Initio* Calculations of Solvated Molecules. *J. Chem. Phys.* **1993**, *97*, 8050.

(44) Senatore, G.; Subbaswamy, K. R. Density Dependence of the Dielectric Constant of Rare-Gas Crystals. *Phys. Rev. B* **1986**, *34*, 5754−5757.

(45) Cortona, P. Direct determination of self-consistent total energies and charge densities of solids: A study of the cohesive properties of the alkali halides. *Phys. Rev. B* **1992**, *46*, 2008−2014.

(46) Shao, X.; Mi, W.; Pavanello, M. GGA-Level Subsystem DFT Achieves Sub-kcal/mol Accuracy Intermolecular Interactions by Mimicking Nonlocal Functionals. *J. Chem. Theory Comput.* **2021**, *17*, 3455.

(47) Mi, W.; Shao, X.; Genova, A.; Ceresoli, D.; Pavanello, M. eQE 2.0: Subsystem DFT beyond GGA functionals. *Comput. Phys. Commun.* **2021**, *269*, 108122.

(48) Mi, W.; Pavanello, M. Nonlocal Subsystem Density Functional Theory. *J. Phys. Chem. Lett.* **2020**, *11*, 272−279.

(49) Schlüns, D.; Klahr, K.; Mück-Lichtenfeld, C.; Visscher, L.; Neugebauer, J. Subsystem-DFT potential-energy curves for weakly interacting systems. *Phys. Chem. Chem. Phys.* **2015**, *17*, 14323−14341.

(50) Laricchia, S.; Fabiano, E.; Constantin, L. A.; Della Sala, F. Generalized Gradient Approximations of the Noninteracting Kinetic Energy from the Semiclassical Atom Theory: Rationalization of the Accuracy of the Frozen Density Embedding Theory for Nonbonded Interactions. *J. Chem. Theory Comput.* **2011**, *7*, 2439−2451.

(51) Götz, A.; Beyhan, S.; Visscher, L. Performance of Kinetic Energy Functionals for Interaction Energies in a Subsystem Formulation of Density Functional Theory. *J. Chem. Theory Comput.* **2009**, *5*, 3161−3174.

(52) Jacob, C.; Visscher, L. In *Recent Progress in Orbital-Free Density Functional Theory*; Wesolowski, T. A., Wang, Y. A., Eds.; World Scientific: Singapore, 2013; pp 299−324.

(53) Krishtal, A.; Sinha, D.; Genova, A.; Pavanello, M. Subsystem Density-Functional Theory as an Effective Tool for Modeling Ground and Excited States, their Dynamics, and Many-Body Interactions. *J. Phys.: Condens. Matter* **2015**, *27*, 183202.

(54) Wesolowski, T. A.; Shedge, S.; Zhou, X. Frozen-Density Embedding Strategy for Multilevel Simulations of Electronic Structure. *Chem. Rev.* **2015**, *115*, 5891−5928.

(55) Neugebauer, J. Chromophore-Specific Theoretical Spectroscopy: From Subsystem Density Functional Theory to Mode-Specific Vibrational Spectroscopy. *Phys. Rep.* **2010**, *489*, 1−87.

(56) Wesolowski, T. A. In *Computational Chemistry: Reviews of Current Trends*; Leszczynski, J., Ed.; World Scientific: Singapore, 2006; Vol. *10*; pp 1−82; .

(57) Jacob, C. R.; Neugebauer, J.; Visscher, L. A Flexible Implementation of Frozen-Density Embedding for Use in Multilevel Simulations. *J. Comput. Chem.* **2008**, *29*, 1011−1018.

(58) Genova, A.; Ceresoli, D.; Krishtal, A.; Andreussi, O.; DiStasio, R., Jr.; Pavanello, M. eQE − A Densitiy Functional Embedding Theory Code For The Condensed Phase. *Int. J. Quantum Chem.* **2017**, *117*, e25401.

(59) Genova, A.; Pavanello, M. Exploiting the Locality of Subsystem Density Functional Theory: Efficient Sampling of the Brillouin Zone. *J. Phys.: Condens. Matter* **2015**, *27*, 495501.

(60) Shao, X.; Umerbekova, A.; Jiang, K.; Pavanello, M. Many-body van der Waals interactions in wet MoS_2 surfaces. *Electronic Structure* **2022**, *4*, 024001.

(61) Witt, W. C.; del Rio, B. G.; Dieterich, J. M.; Carter, E. A. Orbital-free density functional theory for materials research. *J. Mater. Res.* **2018**, *33*, 777−795.

(62) Shao, X.; Mi, W.; Pavanello, M. Efficient DFT Solver for Nanoscale Simulations and Beyond. *J. Phys. Chem. Lett.* **2021**, *12*, 4134−4139.

(63) Witt, W. C.; Shires, B. W. B.; Tan, C. W.; Jankowski, W. J.; Pickard, C. J. Random Structure Searching with Orbital-Free Density Functional Theory. *J. Phys. Chem. A* **2021**, *125*, 1650−1660.

(64) Shao, X.; Jiang, K.; Mi, W.; Genova, A.; Pavanello, M. DFTpy: An efficient and object-oriented platform for orbital-free DFT simulations. *WIREs: Comput. Mol. Sci.* **2021**, *11*, e1482.

(65) Jiang, K.; Pavanello, M. Time-dependent orbital-free density functional theory: Background and Pauli kernel approximations. *Phys. Rev. B* **2021**, *103*, 245102.

(66) Jiang, K.; Shao, X.; Pavanello, M. Nonlocal and nonadiabatic Pauli potential for time-dependent orbital-free density functional theory. *Phys. Rev. B* **2021**, *104*, 235110.

(67) Shin, I.; Ramasubramaniam, A.; Huang, C.; Hung, L.; Carter, E. A. Orbital-free density functional theory simulations of dislocations in aluminum. *Philos. Mag.* **2009**, *89*, 3195−3213.

(68) Chen, M.; Jiang, X.-W.; Zhuang, H.; Wang, L.-W.; Carter, E. A. Petascale Orbital-Free Density Functional Theory Enabled by Small-Box Algorithms. *J. Chem. Theory Comput.* **2016**, *12*, 2950−2963.

(69) Luo, K.; Karasiev, V. V.; Trickey, S. A simple generalized gradient approximation for the noninteracting kinetic energy density functional. *Phys. Rev. B* **2018**, *98*, 041111.

(70) Mi, W.; Pavanello, M. Orbital-free density functional theory Correctly Models Quantum Dots When Asymptotics, Nonlocality and Nonhomogeneity Are Accounted For. *Phys. Rev. B Rapid Commun.* **2019**, *100*, 041105.

(71) Aguado, A.; González, D. J.; González, L. E.; López, J. M.; Núñez, S.; Stott, M. J. *Recent Progress in Orbital-free Density Functional Theory*; World Scientific, 2013; Vol. *6*, pp 55−145; .

(72) Ho, G. S.; Huang, C.; Carter, E. A. Describing metal surfaces and nanostructures with orbital-free density functional theory. *Curr. Opin. Solid State Mater. Sci.* **2007**, *11*, 57−61.

(73) Shao, X.; Mi, W.; Pavanello, M. Revised Huang-Carter nonlocal kinetic energy functional for semiconductors and their surfaces. *Phys. Rev. B* **2021**, *104*, 045118.

(74) Unsleber, J. P.; Dresselhaus, T.; Klahr, K.; Schnieders, D.; Bockers, M.; Barton, D.; Neugebauer, J. Serenity: A subsystem quantum chemistry program. *J. Comput. Chem.* **2018**, *39*, 788−798.

(75) Iannuzzi, M.; Kirchner, B.; Hutter, J. Density Functional Embedding for Molecular Systems. *Chem. Phys. Lett.* **2006**, *421*, 16−20.

(76) Mi, W.; Shao, X.; Genova, A.; Ceresoli, D.; Pavanello, M. eQE 2.0: Subsystem DFT beyond GGA functionals. *Comput. Phys. Commun.* **2021**, *269*, 108122.

(77) Andermatt, S.; Cha, J.; Schiffmann, F.; VandeVondele, J. Combining Linear-Scaling DFT with Subsystem DFT in Born−Oppenheimer and Ehrenfest Molecular Dynamics Simulations: From Molecules to a Virus in Solution. *J. Chem. Theory Comput.* **2016**, *12*, 3214−3227.

(78) Sexton, J. Z.; Kummel, A. C. Comparison of Density Functional Theory Methods as Applied to Compound Semiconductor-Oxide Interfaces: Slab Versus Cluster Models. *J. Vac. Sci. Technol. B* **2003**, *21*, 1908−1914.

(79) Giannozzi, P.; Andreussi, O.; Brumme, T.; Bunau, O.; Nardelli, M. B.; Calandra, M.; Car, R.; Cavazzoni, C.; Ceresoli, D.; Cococcioni, M.; et al. Advanced capabilities for materials modelling with Quantum ESPRESSO. *J. Phys.: Condens. Matter* **2017**, *29*, 465901.

(80) Shao, X.; Andreussi, O.; Ceresoli, D.; Truscott, M.; Baczewski, A.; Campbell, Q.; Pavanello, M. *QEpy: Quantum ESPRESSO in Python*. http://qepy.rutgers.edu. Also available at https://gitlab.com/shaoxc/qepy, 2022.

(81) Chen, M.; Xia, J.; Huang, C.; Dieterich, J. M.; Hung, L.; Shin, I.; Carter, E. A. Introducing {PROFESS} 3.0: An advanced program for orbital-free density functional theory molecular dynamics simulations. *Comput. Phys. Commun.* **2015**, *190*, 228−230.

(82) Shao, X., Mi, W., Pavanello, M. *eDFTpy: An object-oriented platform for density embedding simulations*. Available at http://edftpy.rutgers.edu, 2022.

(83) Pulay, P. Improved SCF Convergence Acceleration. *J. Comput. Chem.* **1982**, *3*, 556−560.

(84) Huang, C.; Carter, E. A. Transferable local pseudopotentials for magnesium, aluminum and silicon. *Phys. Chem. Chem. Phys.* **2008**, *10*, 7109.

▣ Recommended by ACS

Characterizing Molecule–Metal Surface Chemistry with Ab Initio Simulation of X-ray Absorption and Photoemission Spectra

Samuel J. Hall, Reinhard J. Maurer, *et al.*
JANUARY 23, 2023
THE JOURNAL OF PHYSICAL CHEMISTRY C   READ ⬚

XPS Core-Level Chemical Shift by Ab Initio Many-Body Theory

Iskander Mukatayev, Jing Li, *et al.*
FEBRUARY 14, 2023
THE JOURNAL OF PHYSICAL CHEMISTRY A   READ ⬚

Strongly Correlated Electronic Properties of FeO Studied by the SCAN+U Functional

Jingping Dong, Fengjie Ma, *et al.*
MARCH 10, 2023
THE JOURNAL OF PHYSICAL CHEMISTRY C   READ ⬚

A Systematic Theoretical Study on Electronic Interaction in Cu-based Single-Atom Alloys

Guo-Chen Zhao, Chun-Guang Liu, *et al.*
NOVEMBER 04, 2022
ACS OMEGA   READ ⬚

Get More Suggestions >